Skillful multiyear predictions of ocean acidification in the California Current System

Riley X. Brady[1*], Nicole S. Lovenduski[1], Stephen G. Yeager[2], Matthew C. Long[2], Keith Lindsay[2]

[1]Department of Atmospheric and Oceanic Sciences and Institute of Arctic and Alpine Research, University of Colorado, Boulder, Colorado, USA

[2]Climate and Global Dynamics Laboratory, National Center for Atmospheric Research, Boulder, Colorado, USA

*Correspondence to: riley.brady@colorado.edu

Drift Adjustment and Anomaly Generation

Initialized forecasts required drift adjustment due to the use of full-field initialization for the Community Earth System Model Decadal Prediction Large Ensemble[1] (CESM-DPLE). To correct for this model drift, we followed the same procedure as in Yeager et al. 2018. Drift (*i.e.*, lead-time dependent model climatology) was computed as the mean across ensemble members and start dates, separately for each lead time range considered, where only those hindcasts that verify between 1964-2014 are included in the climatology. This drift was then subtracted at each grid cell from all forecasts to generate anomalies. Anomalies were computed for CESM-LE and the reconstruction by subtracting the mean over 1964–2014 at each grid cell. The same was done for the JMA observational product, but over the 1990–2005 period that the CESM-DPLE

forecasts were verified against. A second-order fit was removed from all time series over their verification window.

Model Evaluation

While the JMA observational product spans 1990–2017, the reconstruction loses variability in atmospheric CO_2 forcing from 2005 onwards (Fig. S7A), which causes a drop-off in its ability to replicate observed pH anomalies (Fig. S7B). Thus, we evaluate the reconstruction against the observational product over the 1990–2005 period. The reconstruction provides a good fit to the observational product in terms of the spatial distribution of seasonal surface pH climatologies (Fig. S2). It captures the more basic surface pH during the wintertime downwelling season (Fig. S2A), and progresses toward a peak of more acidic surface pH in the summertime, due to upwelling (Fig. S2C). This matches the spatial progression of surface pH in the JMA observational product (Fig. S2, E to H), as well as high-resolution model solutions [2]. In general, the reconstruction has a slight acidic bias, with a relative mean bias in the hydrogen ion concentration ([H+]) ranging from 2.9% to 4.2% within the CCS Large Marine Ecosystem (Fig. S2, I to L). Over the area-weighted CCS (Fig. S1), the reconstruction simulates a linear change in pH of -0.028 over the 1990–2005 period, compared to the observational product's linear change of -0.030 (Fig. S1A). The reconstruction has a slight mean acidic bias of 0.013 (Fig. S1A), but replicates the seasonal cycle in both phasing and amplitude, with a maximum bias of 0.006 in May, and nearly zero bias from August through November (Fig. S1C). The reconstruction also closely replicates

monthly anomalies (quadratic fit and seasonal cycle removed) from the JMA observational product (Fig. S1B), with a linear correlation coefficient of 0.72, explaining over 50% of the observed variance. In addition to surface pH, previous work has shown that CESM version 1.1 provides a good fit to observational climatology of coastal upwelling, alongshore wind stress, surface pCO_2, and air–sea CO_2 fluxes in the CCS [3,4].

References

1. Yeager, S. G. *et al.* Predicting near-term changes in the Earth system: A large ensemble of initialized decadal prediction simulations using the Community Earth System Model. *Bull. Am. Meteorol. Soc.* **99**, 1867–1886 (2018).
2. Hauri, C. *et al.* Spatiotemporal variability and long-term trends of ocean acidification in the California Current System. *Biogeosciences* **10**, 193–216 (2013).
3. Brady, R. X., Alexander, M. A., Lovenduski, N. S. & Rykaczewski, R. R. Emergent anthropogenic trends in California Current upwelling. *Geophys. Res. Lett.* **44**, 2017GL072945 (2017).
4. Brady, R. X., Lovenduski, N. S., Alexander, M. A., Jacox, M. & Gruber, N. On the role of climate modes in modulating the air–sea CO2 fluxes in eastern boundary upwelling systems. *Biogeosciences* **16**, 329–346 (2019).
5. Hurrell, J. W. *et al.* The Community Earth System Model: A framework for collaborative research. *Bull. Am. Meteorol. Soc.* **94**, 1339–1360 (2013).
6. Danabasoglu, G. *et al.* The CCSM4 ocean component. *J. Clim.* **25**, 1361–1389 (2012).

7. Hunke, E. C., Lipscomb, W. H., Turner, A. K., Jeffery, N. & Elliott, S. CICE: the Los Alamos sea ice model documentation and software user's manual version 4.1 LA-CC-06-012. *T-3 Fluid Dyn. Group Los Alamos Natl. Lab.* **675**, (2010).
8. Lawrence, D. M. *et al.* Parameterization improvements and functional and structural advances in version 4 of the Community Land Model. *J. Adv. Model. Earth Syst.* **3**, (2011).
9. Moore, J. K., Lindsay, K., Doney, S. C., Long, M. C. & Misumi, K. Marine ecosystem dynamics and biogeochemical cycling in the Community Earth System Model [CESM1(BGC)]: Comparison of the 1990s with the 2090s under the RCP4.5 and RCP8.5 Scenarios. *J. Clim.* **26**, 9291–9312 (2013).

Table S1. Model components used for the CESM-DPLE, CESM-LE, and forced ocean—sea ice reconstruction.

Component	Model	Details	Key Reference
Atmosphere	Community Atmosphere Model, version 5 (CAM5)	1° horizontal resolution and 30 vertical levels	Hurrell et al. 2013 [5]
Ocean	Parallel Ocean Program (POP), version 2	1° horizontal resolution and 60 vertical levels	Danabasoglu et al. 2012 [6]
Sea Ice	Community Ice Code (CICE), version 4	Same horizontal grid as the ocean	Hunke and Lipscomb 2008 [7]
Land	Community Land Model (CLM4)	Includes modules for biogeophysics, the hydrological cycle, biogeochemistry, and dynamic vegetation	Lawrence et al. 2011 [8]
Ocean Biogeochemistry	Biogeochemical Elemental Cycling (BEC)	Explicit simulation of carbonate chemistry; three phytoplankton functional types and one zooplankton class; cycling of multiple biogeochemical tracers	Moore et al. 2013 [9]

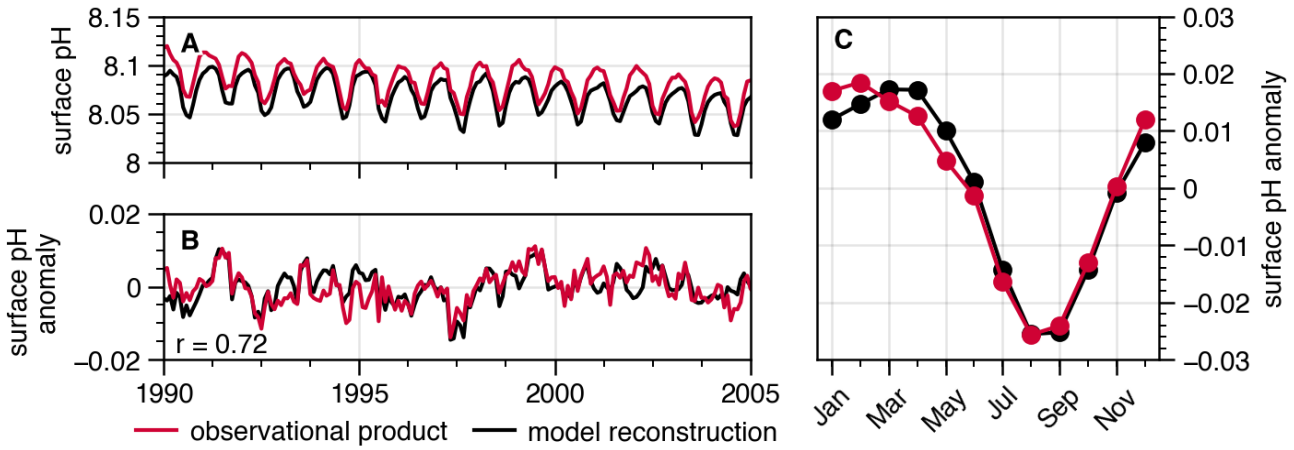

Fig S1. Area-weighted temporal evaluation of surface pH in the model reconstruction. (**A**) Raw surface pH over 1990–2005 for the model reconstruction (black) and observational product (red). (**B**) As in (**A**), but for anomalies after removing a quadratic fit and the seasonal cycle. The correlation coefficient between the observational product and model reconstruction is shown in the bottom left of (**B**). (**C**) As in the other panels, but for the mean seasonal cycle over 1990–2005.

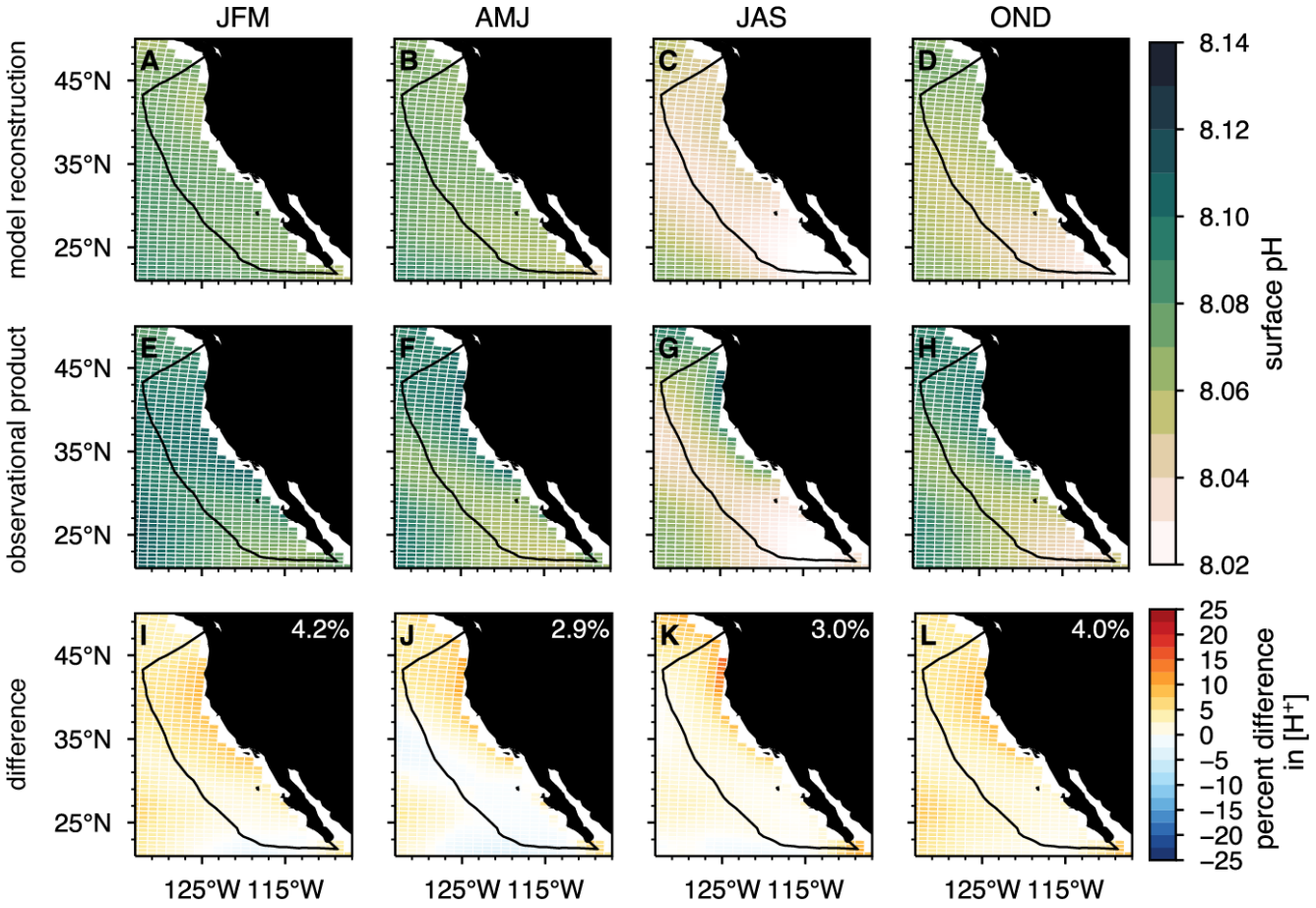

Fig S2. Spatial evaluation of surface pH in the model reconstruction. (**A** to **D**) Seasonal climatology of surface pH for the reconstruction over 1990–2005. Here, the reconstruction is masked to match the missing coastal values in the observational product. (**E** to **H**) As in the previous row, but for the observational product. (**I** to **L**) Bias in the reconstruction as the percent difference in the surface hydrogen ion concentration (positive values indicate an acidic bias in the reconstruction). The percentage in the top right corner of (**I** to **L**) is the mean percent bias within the CCS Large Marine Ecosystem (black outline).

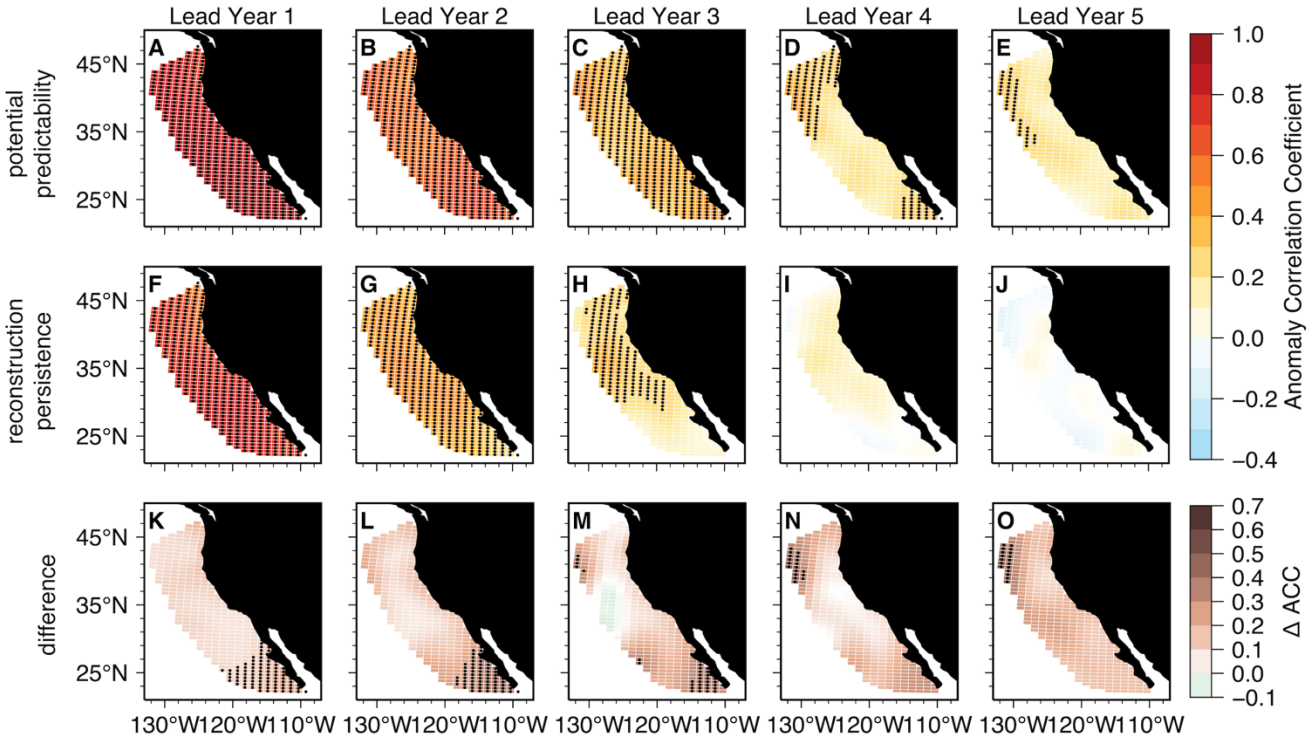

Fig S3. *Potential predictability of salinity-normalized dissolved inorganic carbon (sDIC) in the California Current*. (**A** to **E**) CESM-DPLE initialized forecast of detrended annual surface sDIC anomalies for lead years one through five correlated with the model reconstruction. (**F** to **J**) Persistence forecast for the reconstruction for lead years one through five. Stippling in **A** to **J** denotes statistically significant correlations at the 95% level using a *t* test. (**K** to **O**) Difference between the CESM-DPLE forecast ACCs and persistence. Stippling indicates that the initialized prediction is statistically significant over the persistence forecast at the 95% level using a *z* test. Only positive ACCs and ΔACCs are stippled.

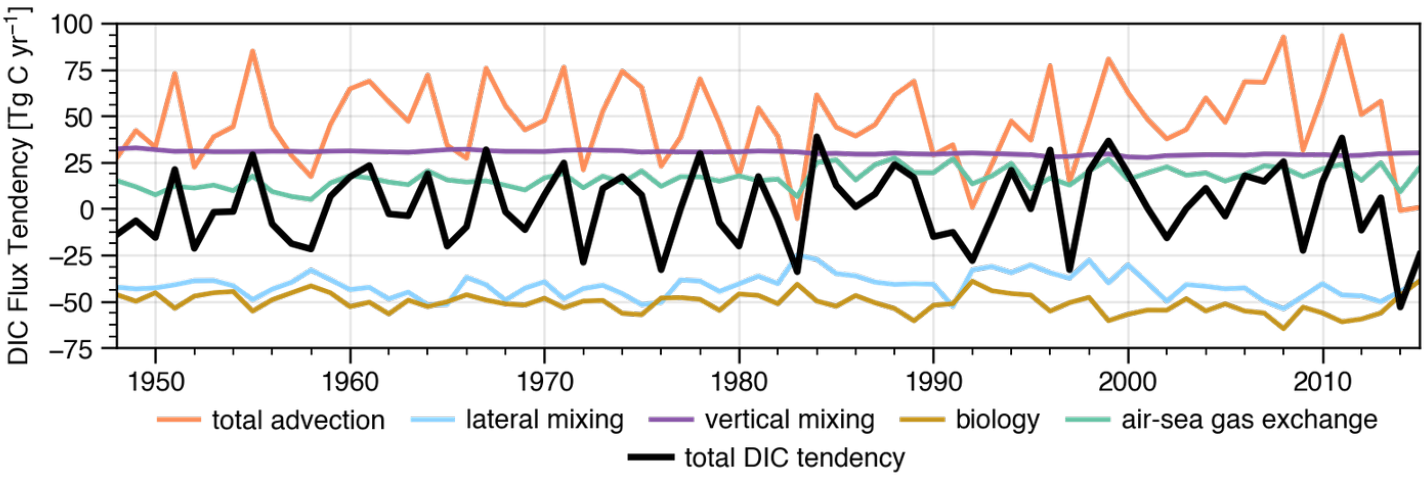

Fig S4. Dissolved inorganic carbon (DIC) budget of the California Current over 150m. Time series of the individual annual tendency terms of DIC in the reconstruction integrated over the CCS laterally and to 150m vertically (the approximate mean mixed layer depth in the model reconstruction). The colored lines show the individual terms, while the thick black line shows the total integrated DIC tendency.

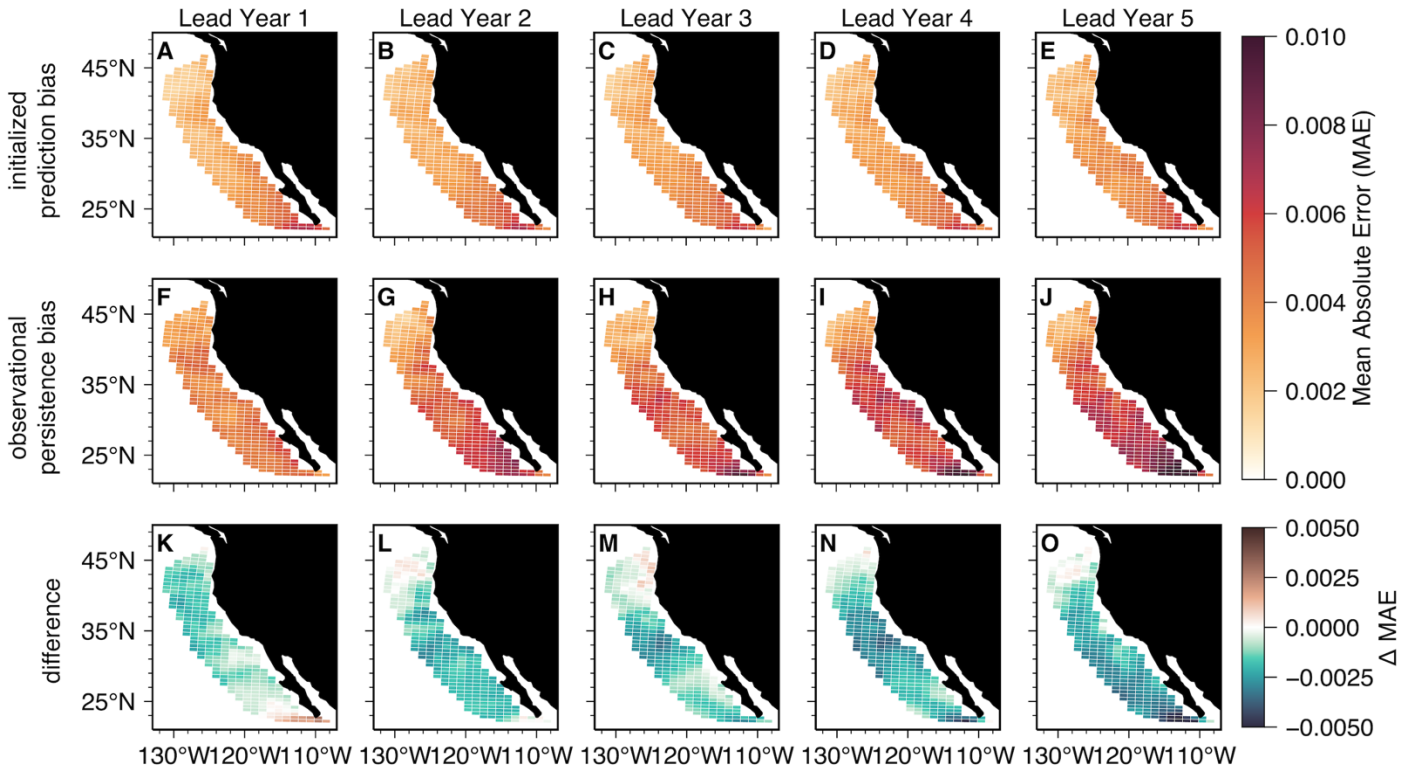

Fig S5. *Bias in predictive skill for surface pH in the California Current*. (**A** to **E**) Mean absolute error (MAE) of CESM-DPLE initialized forecast of detrended annual surface pH anomalies for lead years one through five compared to the observational product. (**F** to **J**) MAE of the persistence forecast for the observational product for lead years one through five. (**K** to **O**) Difference between the CESM-DPLE forecast MAEs and persistence. Blue colors indicate that there is a smaller bias in the initialized forecast than in the persistence forecast.

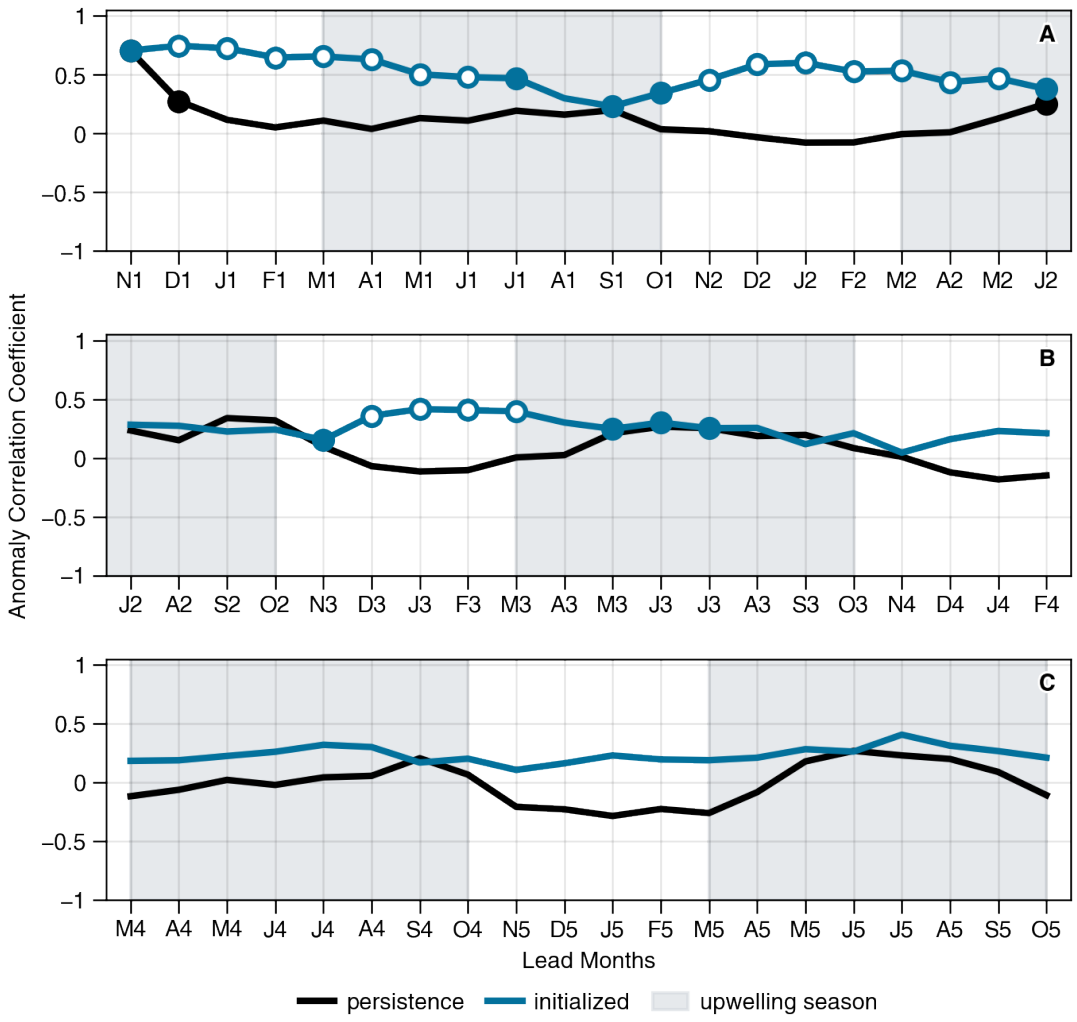

Fig S6. Area-weighted monthly predictability of surface pH in the California Current. The blue line shows the potential predictability by correlating the CESM-DPLE with the reconstruction. The black line shows persistence of the reconstruction. Filled circles denote statistically significant correlations at the 95% level using a t test. White-filled circles denote that the initialized prediction is statistically significant over persistence at the 95% level using a z test. Grey-shaded regions indicate the approximate upwelling season. “N1” indicates the November forecast for the monthly average following initialization, for example.

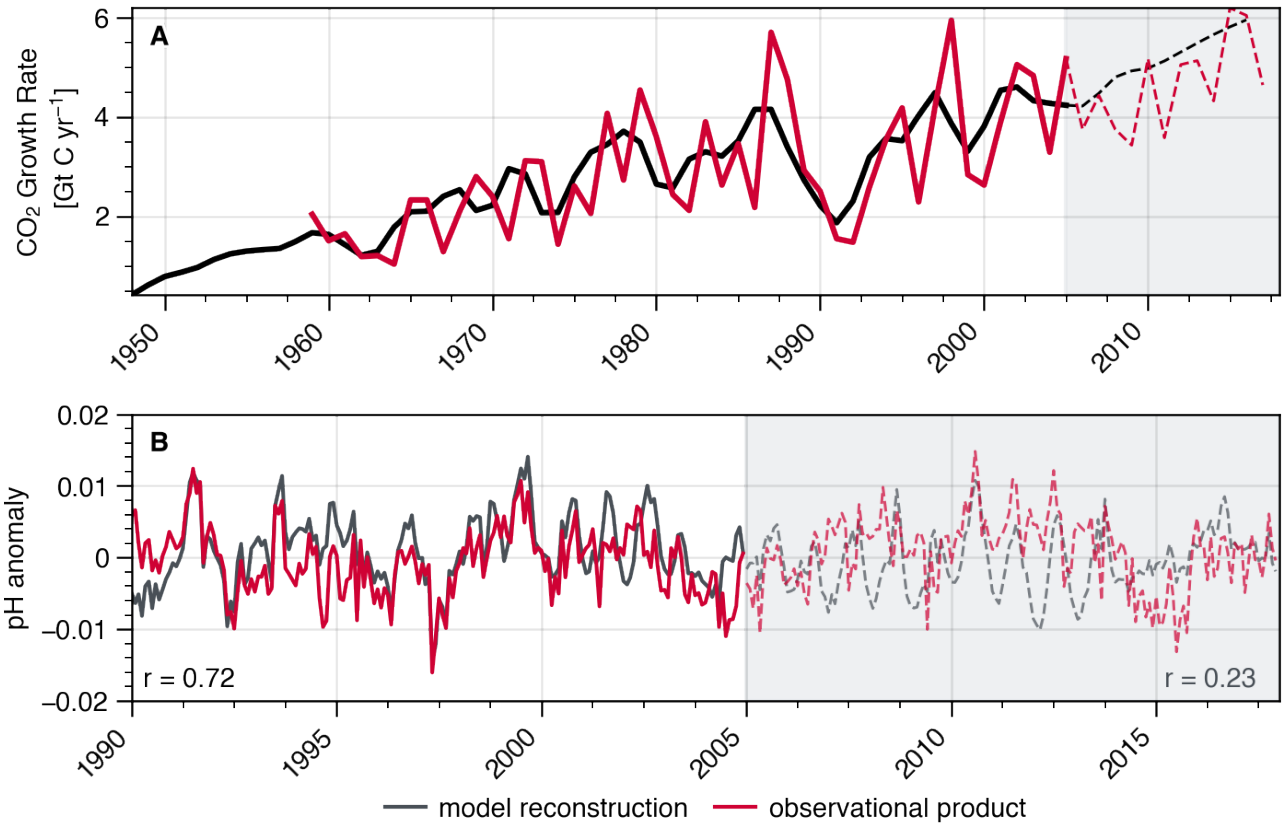

Fig S7. Growth rate of atmospheric CO_2 and monthly anomalies of surface pH in the California Current System. (**A**) Atmospheric CO_2 growth rate from the Global Carbon Project observations (red) and as used for external forcing in the reconstruction (black). (**B**) Surface pH anomalies (quadratic fit and seasonal cycle removed) in the CCS for the reconstruction (black) and observational product (red). The period following 2005 when the reconstruction switches to RCP8.5 forcing (i.e., loses observed atmospheric variability in CO_2) is highlighted in gray. Correlation coefficients between the reconstruction and observational product are shown for the 1990-2005 period (bottom left) and 2006-2017 period (bottom right).